Transportation Infrastructure Geotechnology (2024) 11:263–282
https://doi.org/10.1007/s40515-023-00280-8

TECHNICAL PAPER

Numerical Analysis to Assess the Bearing Capacity of Footings Embedded in Cohesive Soil Slope

Messaoud Baazouzi[1,2] · Boudiaf Khaoula[2] · Tabet Mohamed[1] · Rahmouni Ouassim[3] · Nassima Zatar[4]

Accepted: 16 February 2023 / Published online: 2 March 2023
© The Author(s), under exclusive licence to Springer Science+Business Media, LLC, part of Springer Nature 2023

Abstract

This paper presents a numerical analysis of the centric loading of a strip footing on a cohesive slope. This paper investigates the influence of slope geometry (β), soil strength (C_u), normalized footing distances (λ), and an embedded depth ratio on bearing capacity (D_f/B). These factors are compared with the previous literature. It is evident from the results that slope geometry (β), soil strength (C_u), normalized footing distances (λ), and embedded depth ratio (D_f/B) have significant effects on undrained bearing capacity. The slope creates an unfavorable effect on bearing capacity by reducing the resistance in the passive wedge. Compared to shallow foundations, deeply installed foundations have a much higher ultimate bearing capacity.

Keywords Bearing capacity · Embedded shallow foundation · Failure mechanism · Load · Slope

✉ Messaoud Baazouzi
m.baazouzi@univ-khenchela.dz

Boudiaf Khaoula
boudiafkaoula1@gmail.com

Tabet Mohamed
mohamedx61@gmail.com

Rahmouni Ouassim
rahmouni.ouassim@gmail.com

Nassima Zatar
n.zatar@univ-batna2.dz

[1] Department of Civil Engineering, Faculty of Science and Technology, University of Khenchela, Khenchela, Algeria

[2] Laboratory of Research in Civil Engineering LRGC, University of Biskra, BP14507000 Biskra, Algeria

[3] Department of Civil Engineering, Faculty of Technology, University of Mouloud-Mammeri de Tizi Ouzou, Tizi Ouzou, Algeria

[4] Department of Civil Engineering, Faculty of Technology, University of Batna 2, Batna, Algeria

Symbols

B Footing width
L Footing length
λ Footing distance ratio
λ^* Distance between the base of the footing and the slope face
D_f Embedded depth
q_u The ultimate load of footing near a slope
β° Slope angle
γ Unit weight of soil
φ Internal friction angle
C_u Soil cohesion

1 Introduction

Strip foundations are one of the most cost-effective methods for transmitting loads from light superstructures to the underlying ground. Therefore, bearing capacity is one of the most crucial parameters in designing a strip foundation. It involves a combination of engineering mechanics and the properties of soils. The bearing capacity of a shallow foundation subjected to vertical central loading is typically determined using the bearing capacity equation posed by Terzaghi (1943), expressed as:

$$q_u = \frac{1}{2}B\gamma N_\gamma + cN_c + qN_q \tag{1}$$

where q_u is the ultimate bearing capacity, B is the width of the footing, c is the cohesion, $q = \gamma D_f$, γ is the unit weight of soil and D_f is the embedment depth of the footing, and N_γ, N_c, and N_q are bearing capacity factors.

A wide range of literature has been published on the undrained bearing capacity of strip footings resting on horizontal surfaces: (1) experimental investigations using full-scale tests, laboratory models, and centrifuge models (e.g., Nova and Montrasio 1991; Briaud and Gibbens 1994; Okamura et al. 1997; Badakhshan, Noorzad, and Zameni, 2018); and (2) theoretical and numerical approaches (e.g., Prandtl 1920; Vesic 1973; Anaswara and Shivashankar 2020; Anaswara et al. 2020; Ghazavi and Dehkordi 2021; Alzabeebee 2022; Chen et al. 2022; Fattah et al. 2022; Nalkiashari et al. 2022). However, shallow foundations are located on or near slopes in several situations, especially for bridge abutments, roads, and pylons in mountainous areas (Shields et al. 1990). The bearing capacity may be significantly reduced according to the slope in these cases. Nevertheless, the ultimate bearing capacity is affected by either local foundation failures or global slope failures, which adversely affect the environment in general (Azzouz and Baligh 1983). Many researchers have investigated the issue of strip footings resting near slopes via different approaches, including the limit equilibrium method. Meyerhof (1957) studied the influence of ground surface inclination on bearing capacity factors and proposed design charts that revealed the significant effect of slope on the bearing capacity of a strip footing. Hansen's (1970) expressions were modified semi-empirically by Vesic (1975)

by incorporating corrective factors for the foundation shape, load, and slope of the ground. Based on the slip line method, Kusakabe et al. (1981) and Graham et al. (1988) investigated the bearing capacity of clay slopes under continuous loads. Yang et al. (2019) in their study presented an analytical approach to evaluating the bearing capacity of a shallow foundation near a slope. The results are presented as dimensionless bearing capacity factors (N_{cs}, $N_{\gamma s}$, and N_{qs}), allowing for consideration of the contributions of cohesion, soil weight, and embedment in calculating bearing capacity on slopes. They use traditional bearing capacity factors that comply with current geotechnical practice (e.g., AASHTO 2016). A simple upper-bound limit analysis (UBLA) approach is developed to objectively determine bearing capacity and the associated kinematically admissible mechanisms, either bearing or slope stability failure, for shallow foundations embedded near slopes with c–φ parameters. Chen and Xiao (2020) developed an UBLA method based on the failure mechanisms and bearing capacities of rigid strip footings on cohesionless slopes. They included various slope angles, footing distances from slope crests, slope heights, surcharge footings, and footing depths as part of their comparison. Loading tests have been conducted on model slopes with varying slope angles using 100-mm-wide strip footings (Huang 2019); in experiments, it has been shown that bearing capacity increases when a load is eccentric toward the heel of the footing. In contrast, conventional formulas show the opposite trend. This led to the proposal of a procedure for correcting the bearing capacity of a footing setback from the slope crest to address this discrepancy.

In geotechnical problems, numerical analysis, such as finite element difference and the finite element method, has proven extremely useful in analyzing the complex behavior of stress and strain due to external loading. Shiau and Watson (2008) investigate the finite difference in three-dimensional bearing capacity on homogeneous clay. Georgiadis (2010) employed the finite element method (FEM) and proposed a design procedure for calculating the undrained bearing capacity factor N_c. After that, Shiau et al. (2011) proposed design charts based on averaged lower bound and upper bound results based on the finite element limit analysis method for rough and smooth footings placed on purely cohesive slopes and developed a program to forecast bearing capacity. Discontinuity layout optimization was used to investigate the bearing capacity of the foundation established on a (c'–ϕ') slope by Leshchinsky (2015) and design charts containing critical failure mechanism information by Zhou et al. (2018). Based on a comparison between discontinuity layout optimization (DLO-LA) and the classical ultimate bearing capacity solution, Leshchinsky and Xie (2017) presented design charts in the form of reduction coefficients.

With the rapid development of construction, the existence of slopes may cause the attenuation of the bearing capacity of foundations. Often, engineers design and build the foundation at some depth below the ground's surface. Therefore, it is necessary to place the foundation as far away from the sloped ground as possible to solve the intricate stability problem. However, the literature on the bearing capacity of embedded footings is very inadequate. Therefore, Qian et al. (2019) conducted two full-scale tests on dry low-sloping ground to compare the performance of two straight-sided piers and two belled piers under combined uplift and lateral loads. In addition, using centrifuge

tests, the interaction of reverse faults and shallow foundations embedded at a depth of D_f/B has been evaluated by Ashtiani et al. (2015).

Furthermore, Ko et al. (2018) investigated the differences between the cyclic and dynamic behavior of embedded rocking foundations. Baah and Shukla (2019) investigated the performance of an embedded strip footing on an unreinforced and a single-layer geotextile-reinforced sandy slope by conducting laboratory model tests and finite element analysis. Jiang et al. (2018) established a three-dimensional calculation model to study the behavior of piles on the sloping ground under undrained lateral loading conditions. Han et al. (2020) constructed a numerical model based on field test data to discuss the uplift resistance of foundations embedded in the horizontal ground far from slopes. In non-stationary random soil, Wu et al. (2020) investigate the bearing capacity of embedded shallow foundations in non-stationary random soil, with the mean value increasing linearly with depth and a constant coefficient of variation COV. Their study examines the effects of non-stationary features of soil properties on embedded shallow foundations from three perspectives: failure mechanics, statistical characteristics of the bearing capacity factor, and probability of failure. In addition, Li et al. (2020) used finite element analysis to estimate the ultimate bearing capacity of strip footings placed on slopes. Among the parameters affecting the failure mechanism of the footing-on-slope system, embedded depth and edge distance are more significant than any other parameters. Lai et al. (2022) used a multivariate adaptive regression splines and a pseudo-static technique to evaluate the seismic bearing capacity of footing embedded in cohesive soil slopes.

This study evaluates the influence of various parameters on the undrained bearing capacity of strip footings on or near slopes using the finite-difference code Fast Lagrangian Analysis of Continua (FLAC 2005). The parametric studies presented in this section investigate separately the influence of the five parameters $C_u/(\gamma B)$, D_f/B, β, λ, and λ^*. In addition, a comparison is made between the results of the analyses and the available methods.

2 Problem Definition

Figure 1 shows the geometry of the analyzed problem. This study examines a rigid strip footing of width $B = 1$ m situated on a homogeneous clay soil with angles of $\beta = 15°$, 30°, and 45° and a slope height $H/B = 2$ at several distances from the foundation edge to the slope crest λ and λ^* indicates the distance between the base of the footing and the slope face. Footings are embedded at variable depths (D_f/B). Ratios of D_f/B of 0, 0.5, 1, and 2 were used. With a shear strength C_u, an undrained Young modulus of $E_u =$ 22.5 MPa, a Poisson ratio of $\nu = 0.49$, and an overall soil weight of $\gamma = 18$ kN/m3, the Mohr-Coulomb elastic perfectly plastic constitutive model was used to model the soil as a Tresca material. Footings are assumed to be rigid.

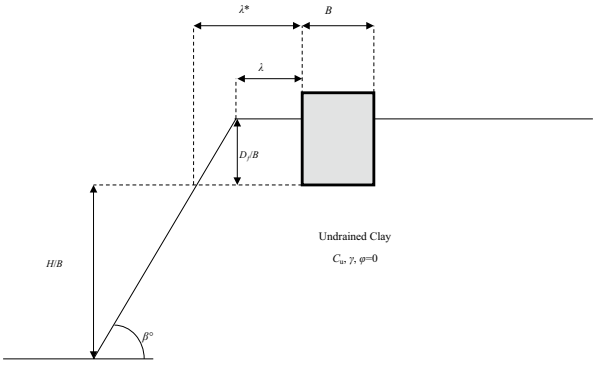

Fig. 1 Problem geometry

3 Numerical Modeling Procedure

A two-dimensional plane-strain finite-difference analysis was performed with Fast Lagrangian Analysis of Continua (FLAC 2005). In engineering mechanics, FLAC (Fast Lagrangian Analysis of Continua) simulates the behavior of structures built out of soil, rock, or other materials that undergo plastic flow when they reach their yield limits by using explicit finite-difference programs. In addition, many researchers have used FLAC to study strip and circular footing-bearing capacities (e.g., Frydman and Burd 1997).

A typical finite element mesh used in the analysis of a $B = 1$ m wide footing at a distance of $\lambda = 1$ m from the crest of a $\beta = 45°$ inclination and a $H/B = 2$ m high soil slope is shown in Fig. 2. To minimize possible boundary effects, the size domain contains 11,999 elements, which corresponds to 42 m × 15 m of wide footing, which minimizes the effects of size (a slight angle of slope of 15° without modifying overall mesh density). The slope was constructed by excavating the appropriate soil layers for each analysis. The mesh dimensions were found to be adequate for the majority of the cases analyzed. To achieve this, different mesh sizes were examined for combinations of geometric properties and materials. Meshes have been refined near the crest of the

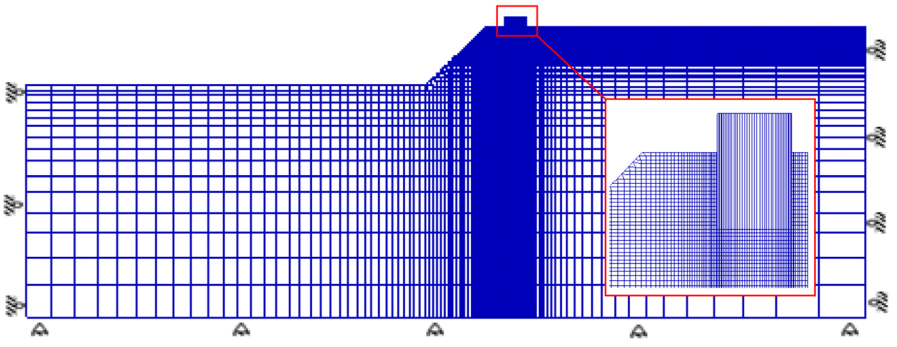

Fig. 2 Finite-difference mesh and boundary condition for the case: $\beta = 45°$, $D_f/B = 1$, and $\lambda = 1$

slope, under the base, and adjacent to the foundation boundaries. In contrast, a larger mesh size indicated that extending the boundaries farther away from the footing did not affect the footing's limit load. The boundary condition for this problem is that the displacement of the left and right vertical sides is constrained horizontally and is fully fixed at the mesh base.

The soil was modeled as a Tresca material using the Mohr-Coulomb elastic perfectly plastic constitutive model with two shear strengths, $C_u = 45$ and 90 KPa, and the undrained Young modulus, $E_u = 22.5$ MPa. In order to model undrained conditions without volume changes and ensure numerical stability, Poisson's ratio was kept constant at $v = 0.49$ (equivalent to a shear modulus of $G = 7.55$ MPa and a bulk modulus of $K = 375$ MPa). A soil's unit weight is $\gamma = 18$ kN/m^3, which affects its overall stability. It was assumed that the footing was made of linear elastic material. It has a concrete Young modulus of $E_c = 29$ GPa and a Poisson ratio of $v = 0.21$. The footing is connected to the soil via interface elements. It is possible to relate the interface elements' properties to the properties of the adjacent soil elements, C_u. Having a normal stiffness K_n of 109 Pa/m and a shear stiffness K_s of 109 Pa/m, these parameters do not substantially impact the failure load.

Numerical modeling consists of the following steps:

- To balance the initial stress, a model of an embedded foundation on a slope was developed, and the original soil in the deep hole was preserved. Then, a gravity value of 10 was applied to the entire soil model.
- The zone representing the footing was subjected to downward velocity (displacement-controlled method). According to conventional calculations, a uniform soil layer causes a progressive movement of the rigid footing caused by vertical velocity applied at the nodes of the footing. This movement is proportional to the distribution of the increase in pressure in the soil. Finally, the pressure under the footing stabilizes at a value that indicates the ultimate vertical load.

Several tests were done to determine the optimal vertical velocity. The value of the velocity applied to the footing area was 1*10–7 m/step. This value is sufficiently small to minimize any inertial effects.

4 Results and Discussions

4.1 Comparison of Available Solutions

4.1.1 Horizontal Ground Surface

In order to verify the reliability predicted by the numerical model, the vertical bearing capacity problem was first validated numerically. Based on Eq. (1), the bearing capacity factor N_c of a strip footing on cohesive soil is as follows:

$$N_c d_c = \left(q_u - q\right)/C_u \tag{2}$$

where N_c is a bearing capacity factor; C_u is a representative undrained shear strength; $q = \gamma D$ is the surcharge at the footing base level; γ is the soil unit weight; D is the distance from the ground surface to the base of the foundation element; and d_c is a depth factor.

Excellent compatibility could be seen between the present simulation results using the $N_c = 5.19$ model and the published data from Prandtl's solution N_c ($= \pi + 2$). The maximum error is 1%, within a reasonable range. It also proves the correctness of the modeling method.

Figure 3 shows the variation of the N_c as a function of the ratio D_f/B compared to those calculated by Edward et al. (2005) and Salgado (2004) for the case of a footing placed on the horizontal ground surface. The gradient of the bearing capacity increased significantly with increasing depth D_f/B, as seen in the graph. For $D_f/B = 0$, the value of N_c obtained from the present study is close to the upper- and lower-bound solutions predicted by Salgado (2004) and the results of Edward (2005). However, it can be seen that the results of Salgado (2004) via the lower-bound solution are slightly more significant than the results of the present study by up to 1.8% for $D_f/B = 1$, while Edward's (2005) solution and the upper-bound solution by Salgado (2004) overestimate the value of N_c by up to 3.30%. Furthermore, for $D_f/B = 2$, the results of Salgado (2004) are shown to be significantly better than the value of N_c determined through the current investigation. However, the upper bound solutions of Salgado's (2004) and Edward's (2005) solutions overestimate the value of N_c by up to 2.48%.

4.2 Parametric Analyses

An investigation of the geometrical characteristics and soil properties is presented in this section. The parametric studies presented in this section investigate separately the influence of the five parameters $C_u/(\gamma B)$, D_f/B, β, λ, and λ^*, specifically $C_u/(\gamma B)$ ratios of 1 and 2.5, three slope angle $\beta = 15°$, 30°, and 45°, and normalized slope/footing distance $\lambda = 0$, 1, 2, 3, 4, 5, 6, 7, 8, 9, and 10. Finally, λ^* corresponds to $[\lambda + (D_f / B) * \cot\beta]$.

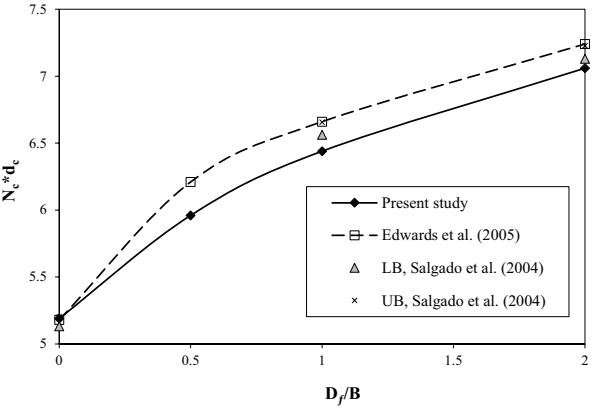

Fig. 3 Comparison of bearing capacity factors of Edward (2005) and Salgado (2004) with the present study

The ultimate bearing capacity would then be stated as

$$N_c = \frac{q_u}{c_u} = f\left(\frac{c_u}{\gamma B}, \beta, \lambda, \lambda^*, \frac{D_f}{B}\right)$$

Additionally, these parameters influence the slope's failure mode, which can occur in any of the four modes described by Zhou et al. (2018), as shown in Fig. 4.

(a-1) The first failure mode is the "face failure mode," which extends along the slope face.

(a-2) Toe failure mode: a failure surface developed from the back corner of the footings to the toe of the slope.

(a-3) Base failure mode: a failure slip extends beneath the toe of the slope, which tends to mobilize a larger volume of shear resistance than face failure and toe failure modes. The passive resistance recovers as the influence of the slope decreases.

(a-4) Prandtl-type failure mode: a general failure mechanism occurs for a footing placed sufficiently far from the slope crest.

"Bearing capacity" failure modes can be referred to as this type of failure. However, the second is as follows:

(b-1) Overall slope failure where the critical shear surface extends beyond the crest and therefore involves part of the slope.

4.2.1 Influence of the Ratio $C_u/(\gamma B)$

A dimensionless strength ratio for slopes with unit weight is defined as $C_u/(\gamma B)$. The unit weight γ plays an essential role in the footing-on-slope problem, unlike the bearing capacity for level ground. Figure 5a shows the effect of the strength ratio $C_u/(\gamma B)$ on the undrained bearing capacity for footing rest on different slope angles $\beta = 15°$, 30°, and 45°, respectively, and for two normalized distances $\lambda = 0$ and 1, where two strength ratios $C_u/(\gamma B) = 1$ and 2.5 are considered. It can be seen that the curves show a decrease in N_c linearly with decreasing strength ratio $C_u/(\gamma B)$, and the depth of the footings until the decrease becomes non-linear due to

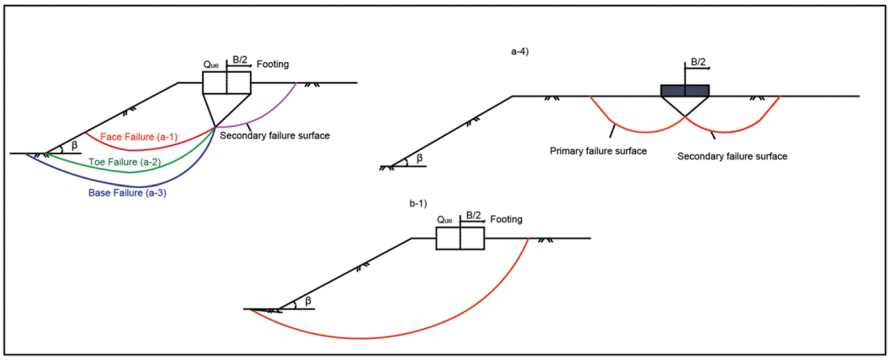

Fig. 4 Different typical failure modes for footing/slope problem (Zhou et al. 2018)

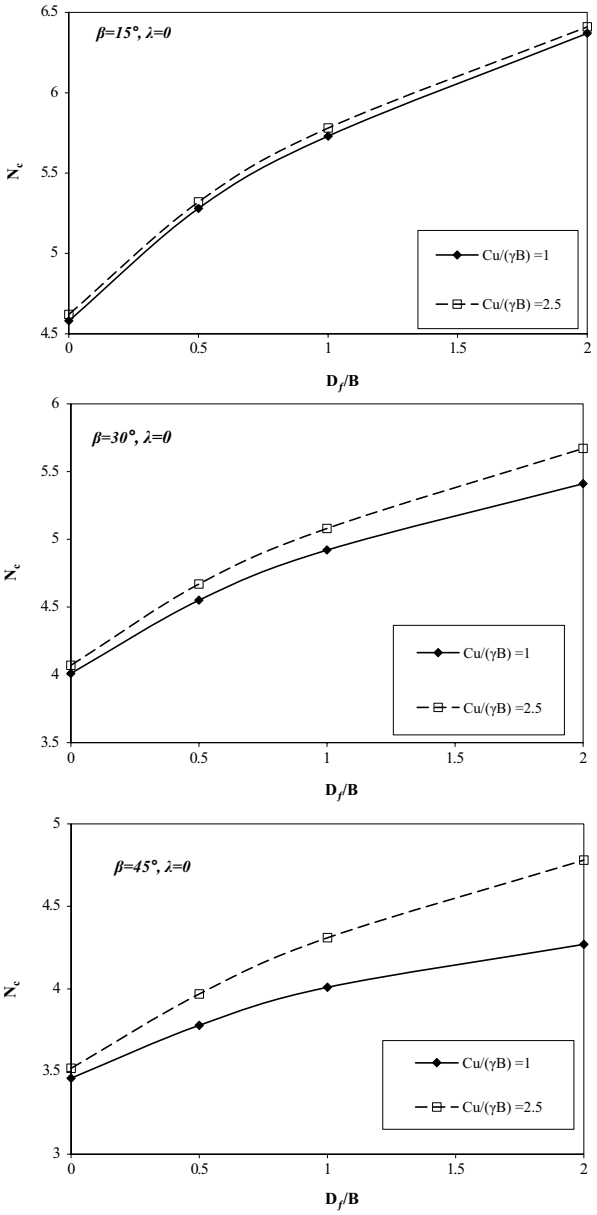

Fig. 5 **a** Variation of N_c for footing at crest of the slope $\lambda = 0$. **b** Variation of d_c for footing at crest of the slope $\lambda = 0$. **c** Contours of maximum shear strain for deep foundation $D_f/B = 1$, $\lambda = 4$, and $\beta = 45°$

the presence of the slopes due to the reduction of passive soil resistance. According to the curves, the linear portion represents failures occurring within the slope face. However, the non-linear part reflects the interplay between the base failure mode and the toe failure mode. As expected, under the same strength ratio, the

Fig. 5 (continued)

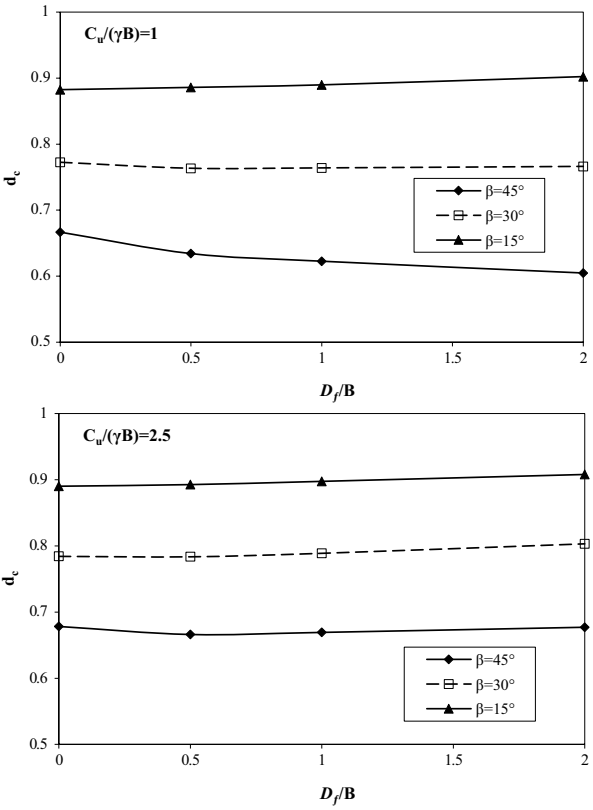

b)

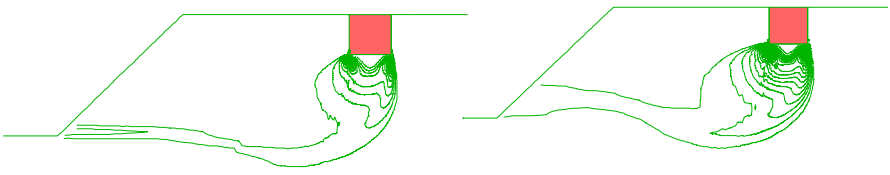

c)

factor N_c increases with a decrease in the slope angle β. Factor N_c increases very rapidly for $\beta = 15°$, while factor N_c increases very slowly for $\beta = 45°$.

For a more intuitive representation of the ratio $C_u/(\gamma B)$, the dimensionless parameter depth factor d_c may be defined as dividing the footings at depth on the sloping ground by those obtained for the surface footing. Figure 5b shows that the dimensionless parameter depth factor d_c continues to increase as the foundation depth D_f/B increases, except for the slope angle $\beta = 45°$. For $C_u/(\gamma B) = 1$, the dimensionless parameter depth factors d_c gradually increase for $\beta = 15°$ as the embedded footing increases, ranging from 0.882 to 0.902, a 20.8% increase. The values for $\beta = 15°$ are

significantly higher than those for other slope angles β. Therefore, the d_c decreases for $\beta = 30°$ before $D_f/B = 0.5$, corresponding to 0.777 and 0.763. Therefore, d_c remains stable throughout the depth D_f/B varying from 0.5 to 2. Consequently, the d_c decreased at a faster rate, a decrease of 9.30% in the range of 0.66–0.60 for $\beta = 45°$. However, when $C_u/(\gamma B) = 2.5$, the dimensionless parameter depth factors d_c increase slowly for $\beta = 15°$ with the increase of embedded footing, varying from 0.88 to 0.90, which increases 20.8%.

The values for $\beta = 15°$ are significantly higher than those for other slope angles β. Therefore, the d_c remains stable for $\beta = 30°$ before $D_f/B = 1$, which is roughly equivalent to 0.77. Subsequently, the d_c increased to 0.80, an increase of 4%. However, d_c decreases in the range of $D_f/B = 0$–0.5 in the field of 0.68–0.66 for $\beta = 45°$, and then slowly increases to 0.68, a 3% increase over the previous value. The dimensionless strength ratio $C_u/(\gamma B)$ effect on the slope angle is much more significant at the lower deep foundation as the slope angle β gets steeper. Some of these failure mechanisms are shown in Fig. 5c for $\beta = 45°$, $\lambda = 4$, and strength ratios $C_u/(\gamma B) = 1$ and 2.5, respectively. It is seen that the contours of the maximum shear strain field of deep footing gradually move away from the toe slope to the face slope with the increase of $C_u/(\gamma B)$.

4.2.2 Effect of the Slope Angle β

The effect of slope angle on the undrained bearing capacity of foundations near a slope can be illustrated in Fig. 6 for $C_u/(\gamma B) = 1$. Since slopes are generally stabilized with an extended embed, the ratio D_f/B varies from 0 to 2. Consequently, the normalized footing distance λ measured from the slope crest varies from 0 to 1. The effect of normalized footing distance λ on the foundation response has also been investigated with varying slope angles, especially considering their values from $\beta = 15°$ to 45°. Meyerhof (1957) revealed that the slope fails because of gravity alone (higher slope angle). This unfavorable effect on bearing capacity can be attributed to reduced resistance in the passive wedge.

It should be noted that $\beta = 0°$ refers to level ground. From Fig. 6a in the case where $\lambda = 0$, it can be observed that an increase in the value of β results in a rapid reduction of the undrained bearing capacity factor, and the slope angle β affects the bearing capacity factor almost linearly. This is because the horizontal ground surface has a more significant undrained bearing capacity factor than near slopes at all foundation depths.

In cases $\lambda = 1$, the bearing capacity decreases as the slope angle increases. However, as the magnitude of β increased, the N_c decrease rate gradually decreased. Considering the behavior of the geometry of the footing, it is clear that the bearing capacity of $\lambda = 0$ is smaller than that of $\lambda = 1$. Furthermore, N_c decreases faster with larger magnitudes of D_f/B. Interestingly, the same N_c factor exists for ratios D_f/B of 0 and 0.5 at = 45°; this indicates that the higher slope angle plays a more active role than the ratio D_f/B.

In order to more intuitively reflect the effect of slope angle, the dimensionless parameter depth factors d_c continue to decrease as slope angle β increases (Fig. 6b).

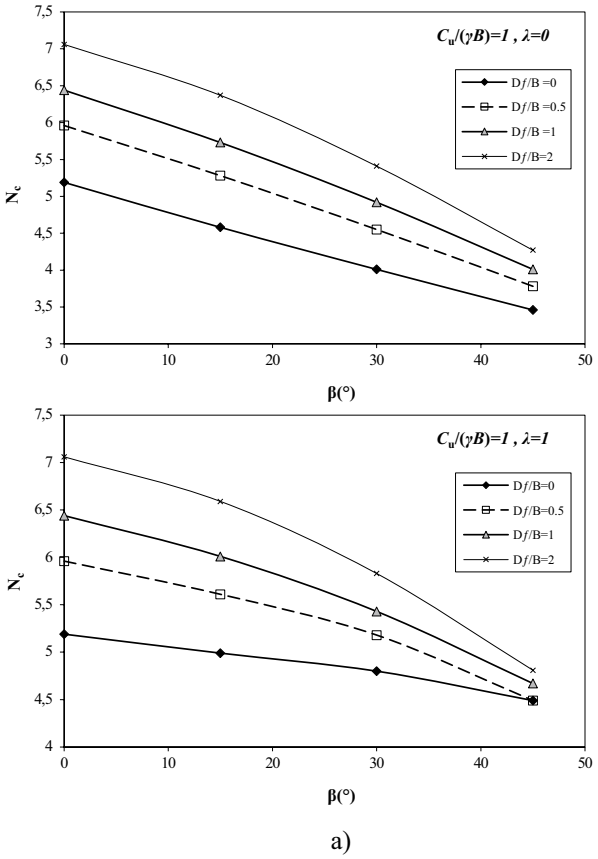

Fig. 6 **a** Variation of N_c with β for $C_u/(\gamma B) = 1$. **b** Variation of d_c for footing at crest of the slope $\lambda = 0$. **c** Contours of maximum shear strain for deep foundation $D_f/B = 2$ and $\lambda = 0$

For $\lambda = 0$, the dimensionless parameter depth factors d_c are identical for embedded footing for $\beta = 15°$ and 30°, respectively. Therefore, the d_c decreases at a faster rate, a decrease of 9.30% in the range of 0.66–0.60 for $\beta = 45°$. However, when $\lambda = 1$, the dimensionless parameter depth factors d_c gradually decrease for $D_f/B = 0$ as the slope angle decreases from 1 to 0.75, increasing by 14%. Therefore, there is a significant difference for $D_f/B = 0.5$ to 2, which increases to 25%, 28%, and 32%, respectively.

Figure 6c illustrates failure mechanisms for $D_f/B = 2$, $\lambda = 0$, and strength ratio $C_u/(\gamma B) = 1$, respectively. As anticipated, it can be seen that the slip surface deepens, and the failure mechanism changes from the Prandtl-type (for footing placed on a horizontal ground surface, $\beta = 0°$). Furthermore, the slip surface expands as the slope angle increases, and the failure mode changes from Prandtl-type failure to face-type failure for small slope angles (less than 30°). It will, however, remain in the toe failure mode ($\beta = 45°$).

Fig. 6 (continued)

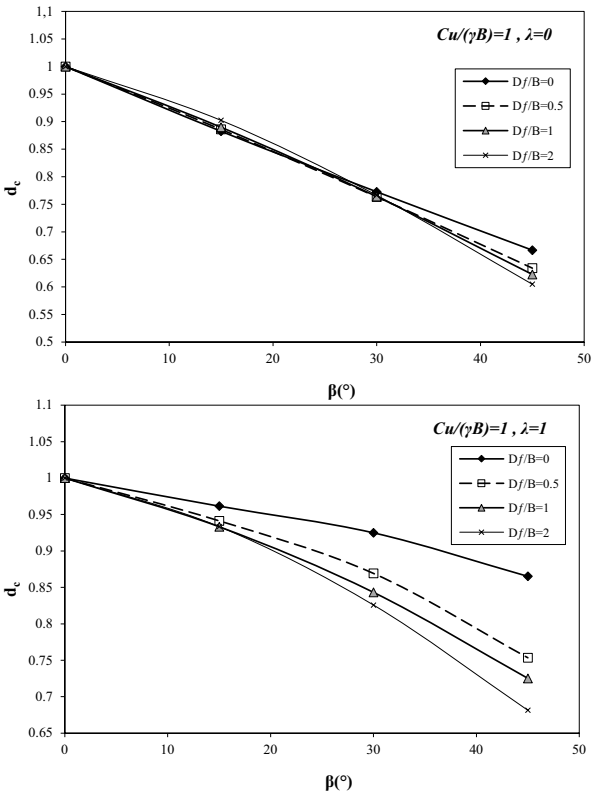

b)

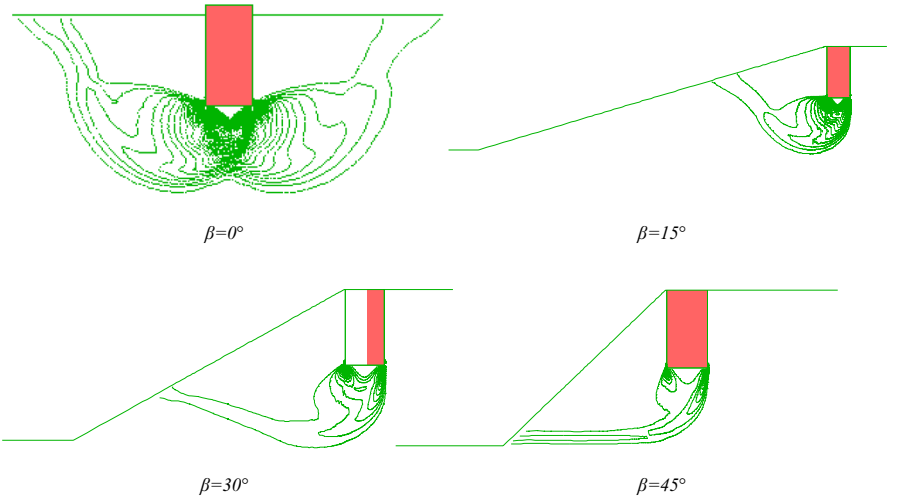

c)

4.2.3 Effect of the Footing Distance to the Crest λ

Figure 7 shows the variation of N_c computed for different footing distances of λ, for slope angles of $\beta = 15°$, 30°, and 45° and $C_u/(\gamma B) = 1$ and 2.5 respectively. It is evident that the λ significantly affects the failure behavior of a footing-on-slope system. As expected, in all cases, the N_c effect is more dominant when the footing is located near the crest of the slope. In parallel, the gradient of each curve indicates that the larger the λ is, the more significant the N_c effect becomes.

In addition, the values of effect-bearing capacity are non-linear in most cases. As the slip surface deepens, the failure mechanism transmits from toe failure to surface failure, eventually obeying Prandtl-type failure. In Prandtl-type failure modes, the N_c factor of the footing remains constant when it is far from the slope crest. The Prandtl-type distance λ_{Prandtl} that results in the bearing capacity of strip footings not influenced by the slope geometry increases with an increase in the embedded depth.

For $D_f/B = 0$, 0.5, 1, and 2, ratio $C_u/(\gamma B) = 1$, the N_c factor reaches a constant value at $\lambda = 1$, 2, 4, and 6 respectively for $\beta = 15°$; $\lambda = 2$, 4, 5, and 7 correspondingly for $\beta = 30°$; and $\lambda = 3$, 4, 7, and 9 accordingly for $\beta = 45°$. The N_c factor, on the other hand, reaches a constant value at $\lambda = 1$, 2, 3, and 4 for $\beta = 15°$; $\lambda = 2$, 3, and 6 for $\beta = 30°$; and $\lambda = 2$, 4, 6, and 8 for $\beta = 45°$. A D_f/B variation from 0.0 to 2.0 increases Prandtl's failure type by 1.36 times.

Edge distance λ^* is a critical variable in a footing-on-slope system's failure behavior. With an increase in the distance ratio λ^*, the footing-on-slope system finally obeys Prandtl-type failure, and the ultimate bearing capacity remains unchanged. With an increased embedded depth, strip footings not influenced by slope geometry will have a higher bearing capacity when they are farthest from the slope. When the embedded depth is not considered ($D_f/B = 0$), the Prandtl-type distance, in this case, is $2\lambda^*$, as mentioned in Fig. 8. Meanwhile, the case's longest Prandtl-type distance is $13\lambda^*$, with the greatest depth $D_f/B = 2$.

Figure 9 shows the variation in the (face failure to toe failure to Prandtl-type failure) mechanism with an increase in the footing distance ratio, which is consistent with the variation in the increased gradient.

5 Conclusion

A finite-difference FLAC (2005) code was used to study the effects of undrained footings on slopes under vertical loads. Analyses were conducted with various geometries and soil properties, and results were compared with other solutions. The slope angle β, the distance of the footing from the slope λ, and the embedded depth D_f/B all play a role in determining the bearing capacity factor N_c. The following conclusions can be drawn based on a detailed analysis of various charts and distinct failure mechanisms:

The unit weight γ plays an extremely significant role in the footing-on-slope problem, unlike the bearing capacity for level ground.

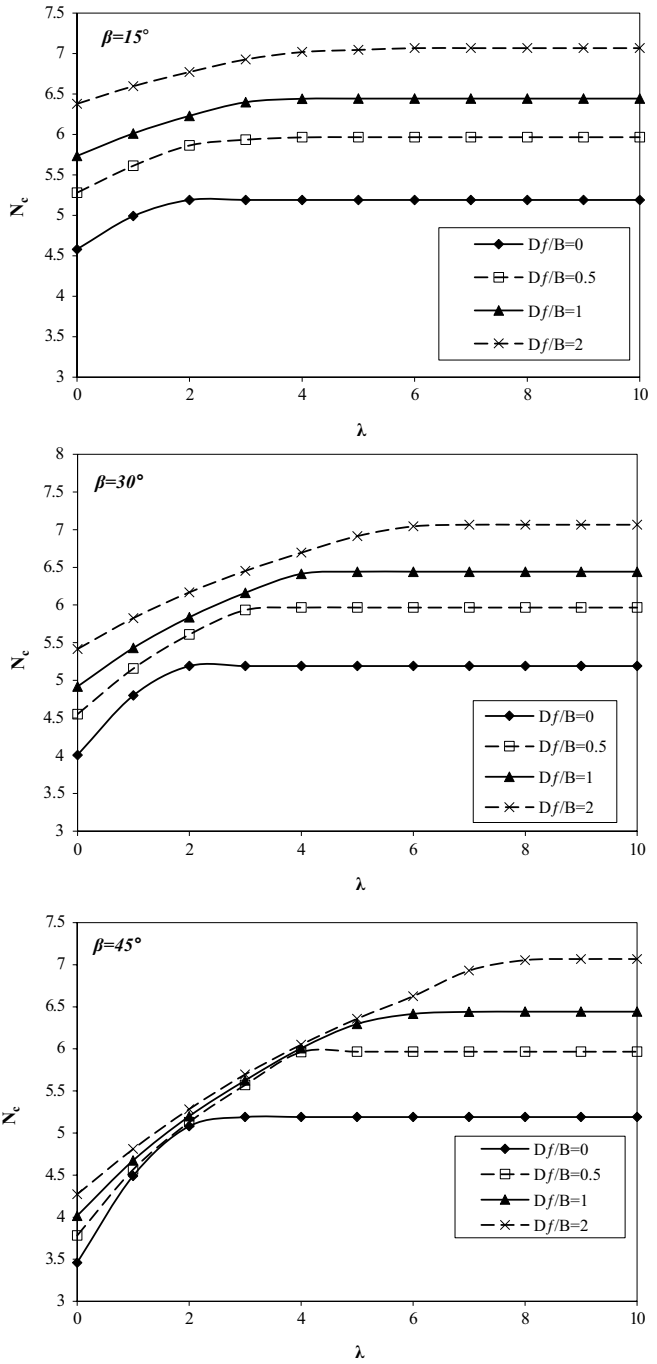

Fig. 7 Variation of N_c with λ for $C_u/(\gamma B) = 1$

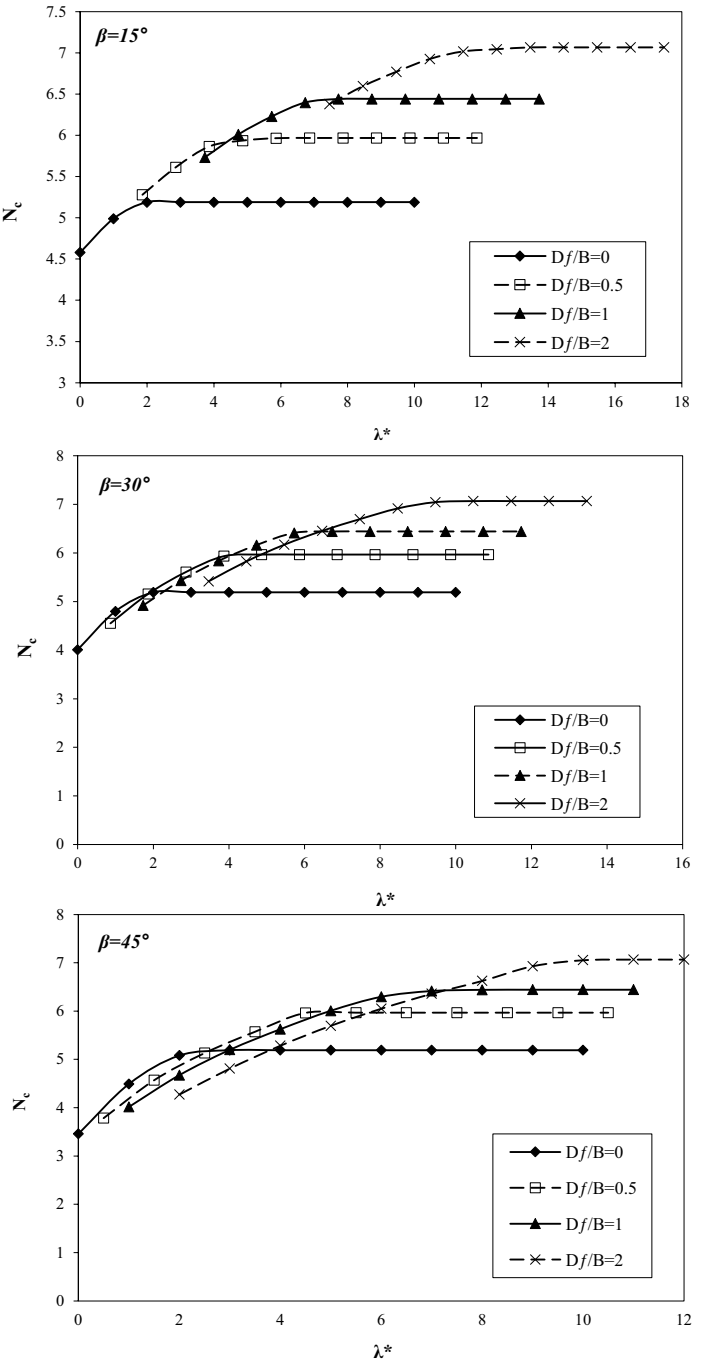

Fig. 8 Variation of N_c with λ^* for $C_u/(\gamma B) = 1$

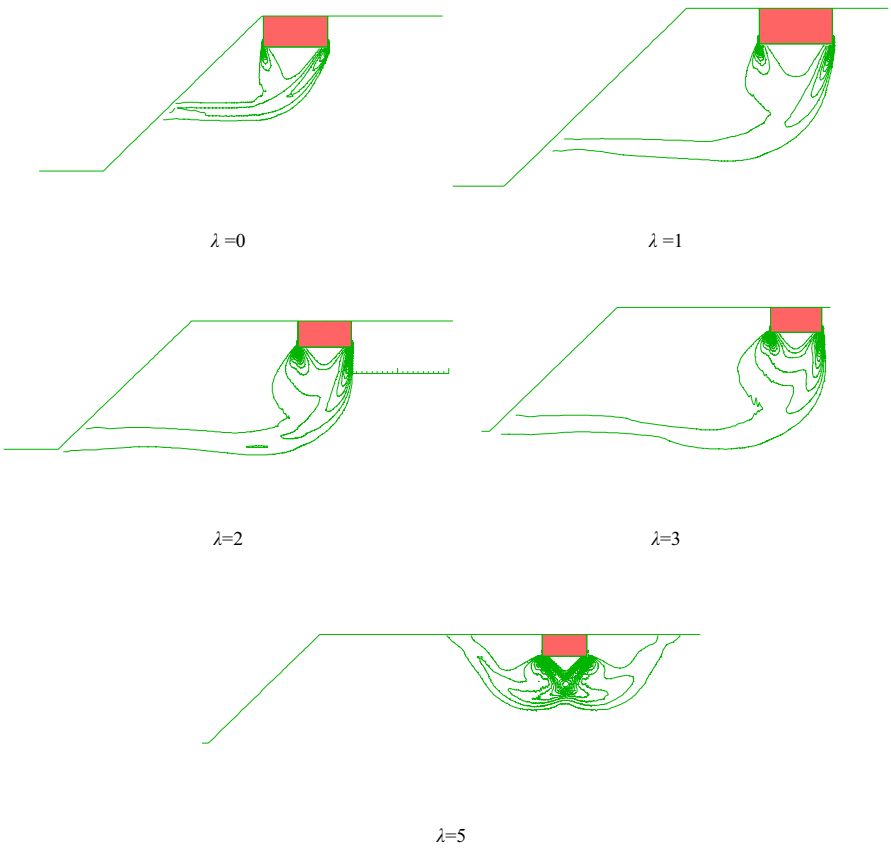

Fig. 9 Contours of maximum shear strain for deep foundation $D_f/B = 1$

As a result, the slope fails due to gravity alone and creates a significant unfavorable effect on the bearing capacity because the passive wedge resists less force.

Undrained bearing capacity N_c increases with increasing strength ratio $C_u/(\gamma B)$. The curves show a decrease in N_c linearly with decreasing strength ratio $C_u/(\gamma B)$, and the depth of the footings until the decrease becomes non-linear due to the presence of the slopes due to the reduction of passive soil resistance. According to the curves, the linear portion represents failures occurring within the slope face. However, the non-linear part reflects the interplay between the base failure mode and the toe failure mode.

The reduction rate in N_c decreased gradually as the magnitude of slope angle β increased. For $\lambda = 0$, the dimensionless parameter depth factors d_c are identical for embedded footing for $\beta = 15°$ and 30°, respectively. Therefore, the d_c decreases at a faster rate, a decrease of 9.30% in the range of 0.66–0.60 for $\beta = 45°$.

Footing distance λ is a significant parameter of the failure behavior of a footing-on-slope system; the bearing capacity factor N_c decreases as footing distance

increases λ. For $D_f/B = 0$, 0.5, 1, and 2, ratio $C_u/(\gamma B) = 1$, the N_c factor reaches a constant value at $\lambda = 1$, 2, 4, and 6 respectively for $\beta = 15°$; $\lambda = 2$, 4, 5, and 7 correspondingly for $\beta = 30°$; and $\lambda = 3$, 4, 7, and 9 accordingly for $\beta = 45°$. The N_c factor, on the other hand, reaches a constant value at $\lambda = 1$, 2, 3, and 4 for $\beta = 15°$; $\lambda = 2$, 3, and 6 for $\beta = 30°$; and $\lambda = 2$, 4, 6, and 8 for $\beta = 45°$. A D_f/B variation from 0.0 to 2.0 increases Prandtl's failure type by 1.36 times.

Prandtl-type failure is the expected failure mode for footings on horizontal ground surfaces. As the slope angle β increases, the slip surface expands, and the failure mechanism changes from the Prandtl-type failure mode to the face failure mode or the toe failure mode.

Acknowledgements We would like to acknowledge the team of LRGC Biskra.

Author Contribution Baazouzi Messaoud acquired methodology and contributed to the investigation, data curation, and writing—original draft.
Boudiaf Khaoula acquired software and contributed to the investigation and data curation.
Tabet Mohamed contributed to writing—reviewing and editing.
Rahmouni Ouassimc contributed to writing—reviewing and editing.
Nassima Zatar contributed to reviewing and editing.

Funding This study was supported by the University of Khenchela and the Laboratory of Research in Civil Engineering, Biskra.

Data Availability All data, models, or codes supporting this study's findings are available from the corresponding author upon reasonable request.

Declarations

Ethics Approval and Consent to Participate All respondents gave consent to participate in the survey.

Consent for Publication Not applicable

Competing Interests The authors declare no competing interests.

References

Alzabeebee, S.: Interference of surface and embedded three strip footings in undrained condition. Transp Infrastruc Geotechnol. **9**(2), 250–267 (2022)
Anaswara, S., Shivashankar, R.: Study on behaviour of two adjacent strip footings on granular bed overlying clay with a void. Transp Infrastruc Geotechnol. **7**(3), 461–477 (2020)
Anaswara, S., Lakshmy, G.S., Shivashankar, R.: Interference studies of adjacent strip footings on unreinforced and reinforced sands. Transp Infrastruc Geotechnol. **7**, 535–561 (2020)
Ashtiani, M., Ghalandarzadeh, A., Towhata, I.: Centrifuge modeling of shallow embedded foundations subjected to reverse fault rupture. Can Geotech J. **53**(3), 505–519 (2015)
Azzouz, A.S., Baligh, M.M.: Loaded areas on cohesive slopes. J Geotech Eng. **109**(5), 724–729 (1983)
Baah-Frempong, E., Shukla, S.K.: Embedded strip footing in a geotextile reinforced sand slope. Proc Inst of Civ Engineers-Ground Improvement. **174**(2), 116–31 (2021)
Badakhshan, E., Noorzad, A., Zameni, S.: Eccentrical behavior of square and circular footings resting on geogrid-reinforced sand. Intl J Geotech Eng. **14**(2), 151–161 (2020)
Briaud, J.L., Gibbens, R.M.: Predicted and measured behavior of five spread footings on sand. ASCE LIBRARY (1994)

Chen, T., Xiao, S.: An upper bound solution to undrained bearing capacity of rigid strip footings near slopes. Intl J Civ Eng. **18**(4), 475–485 (2020)
Chen, H., Zhu, H.: & Zhang, L: An analytical approach to the ultimate bearing capacity of smooth and rough strip foundations on rock mass considering three-dimensional (3D) strength. Comput Geotech **149**, 104865 (2022)
Edwards, D., Zdravkovic, L., Potts, D.: Depth factors for undrained bearing capacity. Géotechnique **55**(10), 755–758 (2005)
Fattah, M.Y., Karim, H.H., Al-Qazzaz, H.H.: Effect of embedment depth on cyclic behavior of tank footings on dry sand. Transp Infrastruc Geotechnol. **9**(2), 220–235 (2022)
FLAC.: Fast Lagrangian Analysis of Continua, version 5.0. ITASCA Consulting Group, Inc., Minneapolis (2005)
Frydman, S., Burd, H.J.: Numerical studies of bearing-capacity factor N_γ. J Geotech Geoenviron Eng **123**(1), 20–29 (1997)
Georgiadis, K.: Undrained bearing capacity of strip footings on slopes. J Geotech Geoenviron Eng **136**(5), 677–685 (2010)
Ghazavi, M., Dehkordi, P.F.: Interference influence on behavior of shallow footings constructed on soils, past studies to future forecast: a state-of-the-art review. Transp Geotech. **27**, 100502 (2021)
Graham, J., Andrews, M., Shields, D.H.: Stress characteristics for shallow footings in cohesionless slopes. Can Geotech J. **25**(2), 238–249 (1988)
Han, Y., Cheng, J., Zheng, W., Ding, S.: Estimating the uplift bearing capacity of belled piers adjacent to sloping ground by numerical modeling based on field tests. Advances in Civil Engineering. 1-12 (2020)
Hansen, J. B.: A revised and extended formula for bearing capacity. Bulletin No. 28, Danish Geotechnical Institute, Copenhagen, Denmark (1970)
Huang, C.-C.: Effects of restraining conditions on the bearing capacity of footings near slopes. Soils and Foundations. **59**(1), 1–12 (2019)
Jiang, C., He, J.-L., Liu, L., Sun, B.-W.: Effect of loading direction and slope on laterally loaded pile in sloping ground. Advances in Civil Engineering. 1-12 (2018)
Ko, K.-W., Ha, J.-G., Park, H.-J., Kim, D.-S.: Comparison between cyclic and dynamic rocking behavior for embedded shallow foundation using centrifuge tests. Bull Earthq Eng. **16**(11), 5171–5193 (2018)
Kusakabe, O., Kimura, T., T., Yamaguchi, H.: Bearing capacity of slopes under strip loads on the top surfaces. Soils and Foundations. **21**(4), 29–40 (1981)
Lai, V.Q., Lai, F., Yang, D., Shiau, J., Yodsomjai, W., Keawsawasvong, S.: Determining seismic bearing capacity of footings embedded in cohesive soil slopes using multivariate adaptive regression splines. Intl J Geosynth Ground Eng. **8**(4), 1–18 (2022)
Leshchinsky, B.: Bearing capacity of footings placed adjacent to c′-ϕ′ slopes. J Geotech Geoenviron Eng. **41**(6), 04015022 (2015)
Leshchinsky, B., Xie, Y.: Bearing capacity for spread footings placed near c′-ϕ′ slopes. J Geotech Geoenviron Eng. **143**(1), 06016020 (2017)
Li, C., Zhou, A., Jiang, P.: Eccentric bearing capacity of embedded strip footings placed on slopes. Comput Geotech. **119**, 103352 (2020)
Meyerhof, G.: The ultimate bearing capacity of foundations on slopes. In Proc., 4th Int. Conf. on Soil Mechanics and Foundation Engineering, London. 1, 384–386 (1957).
Nalkiashari, L.A., Firouzeh, S.H., Payan, M., Chenari, R.J., Shafiee, A.: Interaction of rigid shallow foundation with dip-slip normal fault rupture outcrop: effective parameters and retrofitting strategies. Comput Geotech. **149**, 104866 (2022)
Nova, R., Montrasio, L.: Settlements of shallow foundations on sand. Géotechnique. **41**(2), 243–256 (1991)
Okamura, M., Takemura, J., Kimura, T.: Centrifuge model tests on bearing capacity and deformation of sand layer overlying clay. Soils and Foundations. **37**(1), 73–88 (1997)
Prandtl, L.: Über die härte plastischer körper, pp. 74–85. Nachrichten von der Gesellschaft der Wissenschaften zu Göttingen, Mathematisch Physikalische Klasse (1920)
Qian, Z.-Z., Lu, X.-L., Yang, W.-Z.: Comparative field tests on straight-sided and belled piers on sloping ground under combined uplift and lateral loads. J Geotech Geoenviron Eng. **145**(1), 04018099 (2019)
Salgado, R., Lyamin, A., Sloan, S., Yu, H.: Two-and three-dimensional bearing capacity of foundations in clay. Géotechnique. **54**(5), 297–306 (2004)

Shiau, J., S., Merifield. R. S., Lyamin. A.V., Sloan.S.W.: Undrained stability of footings on slopes. Int. J. Geomech; ASCE. 11, 381-390 (2011)
Shiau, J., Watson, J.: 3D bearing capacity of shallow foundations located near deep excavation sites. Paper presented at the Proceedings of the 2008 International Conference on Deep Excavation (ICDE 2008). Singapore 10-12 (2008)
Shields, D.H., Chandler, N., Garnier, J.: Bearing capacity of foundation in slopes. J Geotech Eng, ASCE. **116**, 528–537 (1990)
Terzaghi, K.: Theory of consolidation, pp. 265–296. Theoretical Soil Mechanics, John Wiley and Sons Inc, New York, USA (1943)
Vesic, A.S.: Analysis of ultimate loads of shallow foundations. J Soil Mech Foundations Division **99**(sm1), 45–73 (1973)
Vesic. A. S.: Bearing capacity of shallow foundations. In: Winterkorn HF, Fang HY, editors. Foundation engineering handbook. Van Nostrand Reinhold (1975)
Wu, G., Zhao, H., Zhao, M., Xiao, Y.: Undrained seismic bearing capacity of strip footings lying on two-layered slopes. Comput Geotech. **122**, 103539 (2020)
Wu, Y., Zhou, X., Gao, Y., Shu, S.: Bearing capacity of embedded shallow foundations in spatially random soils with linearly increasing mean undrained shear strength. Comput Geotech. 122, 103508 (2020)
Yang, S., Leshchinsky, B., Cui, K., Zhang, F., Gao, Y.: Unified approach toward evaluating bearing capacity of shallow foundations near slopes. J Geotech Geoenviron Eng. **145**(12), 04019110 (2019)
Zhou, H., Zheng, G., Yin, X., Jia, R., Yang, X.: The bearing capacity and failure mechanism of a vertically loaded strip footing placed on the top of slopes. Comput Geotech. **94**, 12–21 (2018)

Publisher's Note Springer Nature remains neutral with regard to jurisdictional claims in published maps and institutional affiliations.

Springer Nature or its licensor (e.g. a society or other partner) holds exclusive rights to this article under a publishing agreement with the author(s) or other rightsholder(s); author self-archiving of the accepted manuscript version of this article is solely governed by the terms of such publishing agreement and applicable law.